Evaluation of an electrospun nanocellulose composite membrane for potential vascular tissue engineering applications

Thomas Fruleux, Hanyuan Chen, Jiemin Wang, Mizi Fan, Catalina Vallejo-Giraldo, Manus Biggs

PII: S2772-9508(26)00144-5

DOI: https://doi.org/10.1016/j.bioadv.2026.214846

Reference: BIOADV 214846

To appear in:

Received date: 15 January 2026

Revised date: 16 March 2026

Accepted date: 25 March 2026

Please cite this article as: T. Fruleux, H. Chen, J. Wang, et al., Evaluation of an electrospun nanocellulose composite membrane for potential vascular tissue engineering applications, (2024), https://doi.org/10.1016/j.bioadv.2026.214846

Evaluation of an Electrospun Nanocellulose Composite Membrane for potential Vascular Tissue Engineering Applications

Thomas Fruleux[1], Hanyuan Chen[2], Jiemin Wang[1], Mizi Fan[2], Catalina Vallejo-Giraldo[1] and Manus Biggs[1*]

[1] CURAM, SFI Research Centre for Medical Devices, University of Galway, Galway, Ireland

[2] Nanocellulose and Biocomposites Research Centre, Brunel University of London, UB8 3PH, United Kingdom

Correspondence: Pr. Manus Biggs

CÚRAM, SFI Research Centre for Medical Devices, University of Galway, Galway, Ireland

Post code: H91 W2TY

E-mail address: manus.biggs@universityofgalway.ie

ABSTRACT

Cellulose, the most abundant biopolymer on Earth, offers a sustainable alternative to synthetic materials in biomedical applications. Among cellulose-derived materials, nanocellulose has attracted increasing attention due to its favourable biocompatibility, versatility, and compatibility with advanced fabrication techniques such as electrospinning, 3D printing, and freeze-drying. In this study, Polystyrene/nanocellulose composite membranes fabricated via electrospinning were produced and systematically characterized, and their cytocompatibility was comparatively evaluated against solvent-cast nanocellulose membranes and standard tissue culture plates.

Comprehensive morphological and physicochemical analyses were performed, followed by cytocompatibility evaluations using primary human umbilical vein endothelial cells (HUVECs). Cell viability, proliferation, inflammatory response, and qualitative endothelial layer formation were evaluated over a 21-day culture period. HUVEC proliferation and viability on electrospun membranes were comparable to those observed on solvent-cast nanocellulose membranes and standard tissue culture plates (TCP) after 21 days. All membrane formulations exhibited a reduction in reactive oxygen species over time, while electrospun membranes demonstrated a more homogenous cytokine expression profile (IL-6, IL-23, IFN-α2, and TNF-α) during long-term culture. However, qualitative assessment of endothelial layer formation indicated a delayed development of a mature endothelial monolayer on electrospun membranes compared with solvent cast membranes and tissue culture controls.

Overall, these findings demonstrate the cytocompatibility of electrospun nanocellulose composite membranes and highlight how differences in fabrication strategy and resulting membrane characteristics influence endothelial cell responses. This study provides a comparative and exploratory evaluation of nanocellulose composite membrane systems, supporting their further consideration as sustainable biomaterial for vascular-related biomedical research.

Keywords: Nanocellulose; Electrospinning; Endothelial Cells; Cytocompatibility; Vascular Grafts; HUVECs; Sustainable Biomaterials

1. INTRODUCTION

Cardiovascular diseases remain the leading cause of morbidity and mortality worldwide, creating a sustained clinical demand for functional vascular grafts and artificial blood vessels [1]. Although large-diameter vascular prostheses have achieved considerable clinical success, the development of small-diameter vascular grafts (<6 mm) remains a major bioengineering challenge [2]. Current grafts frequently suffer from thrombosis, intimal hyperplasia, and insufficient endothelialization, ultimately leading to graft failure [3]. As a result, vascular tissue engineering has emerged as a promising strategy to fabricate biomaterials that better recapitulate the structural, mechanical, and biological features of native blood vessels [4], with particular emphasis on promoting endothelial cell adhesion, proliferation, and long-term functional stability [5].

Significant advances have been made in vascular tissue engineering through the use of both synthetic and natural biomaterials [6]. Synthetic polymers such as expanded polytetrafluoroethylene (ePTFE), polyethylene terephthalate (PET), and polyurethanes offer favourable mechanical strength and manufacturability; however, their limited bioactivity and poor endothelialisation often compromise long-term performance, particularly in small-diameter applications [3, 6]. Natural polymers, including collagen, gelatine, and silk fibroin, provide enhanced biocompatibility and cell-interactive properties, but frequently suffer from insufficient mechanical robustness, batch-to-batch variability, and limited structural tunability [6,7]. Moreover, increasing environmental concerns and sustainability considerations highlight the need for renewable and biodegradable alternatives to conventional petroleum-based materials [6,7]. Consequently, there is a growing interest in biomaterials that can simultaneously support endothelial cell function, enable precise structural control, and meet emerging sustainability requirements [8].

Nanocellulose (NC) represents the most abundant natural polymer on Earth, extracted primarily from the plant cell wall [9,10]. Its high stiffness, large surface area, and abundance of hydroxyl groups, facilitate chemical functionalization and implicate NC as an ideal candidate for a wide range of applications, including energy storage [11,12], automotive [13], textiles [14], and biomedical devices [15–17].

Nanocellulose can be derived through both bottom-up and top-down approaches, allowing customization of material properties for specific applications [18]. The major types of nanocellulose derivatives include plant-derived cellulose nanocrystals (CNC), cellulose nanofibres (CNF), as well as bacterial nanocellulose (BNC). Although these materials share a similar biochemical composition, they differ significantly in structural and functional properties.

CNC and CNF, typically extracted from wood pulp or agricultural residues, offer a higher aspect ratio and surface accessibility, enabling strong interactions with the surrounding microenvironment. Their plant-based origin and cost-effectiveness also support circular economy strategies and ecological sustainability. Besides, CNC and CNF offer better structure control and processing versatility owing to their biomass origin. In contrast, BNC, synthesized by certain bacterial species, is characterized by its high crystallinity, mechanical strength, and purity—lacking the hemicellulose and lignin typically present in CNC and CNF [19,20]. It forms a highly organized 3D nanofibre network, influenced by oxygen availability and bacterial activity during biosynthesis [21], presenting challenges for controlling the final structure.

Nanocellulose-based biomaterials are emerging as promising candidates for the next generation of biomedical devices. Their biocompatibility, structural tunability, and environmental friendliness align with the growing demand for sustainable medical solutions [22]. Promoting the use of nanocellulose as a substitute for the conventional petroleum-based materials has the potential to positively impact the life-cycle assessment of current membrane technologies and improve end-of-life management of human waste in biomedical laboratories by fostering circularity and biodegradability [22,23].

Within the biomedical sector, vascular grafts and artificial blood vessels represent a particularly promising application. Several studies have highlighted the favourable cytocompatibility and hemocompatibility of BNC-based materials in vascular tissue engineering. For instance, Lin et al. [24] demonstrated that the surface microstructure and elastic modulus of BNC scaffolds significantly influence endothelial cell behaviour and platelet adhesion. Bao et al. [21] also showed that fibre density and entanglement in BNC scaffolds affect the proliferation and differentiation of human umbilical vein endothelial cells (HUVECs), particularly in oxygen-regulated microenvironments.

Plant-based nanocellulose, i.e. CNC and CNF, represents an excellent candidate for the generation of nanocomposite biomaterials, with particular utility in dynamic application such as engineered blood vessels or heart valves. Additionally, their open network structure offers greater hydroxyl group accessibility, allowing for easier surface functionalization compared to BNC [25]. For example, Bernier et al. [26] observed enhanced red blood cell interactions without any aggregation when surrounded by cationic cellulose nanocrystals, although care must be taken to avoid proinflammatory responses due to variations in nanoparticle shape and hydroxyl density [27]. Despite numerous in vitro studies on plant-based nanocellulose interactions with epithelial cells [28–31], their effects on endothelial cells remain underexplored.

Recent studies have explored versatile fabrication techniques in the formulation of various cellulose-derived biomaterials, including 3D printing, freeze drying, and electrospinning. Among these manufacturing processes, electrospinning promotes the fabrication of nanofibrous scaffold that can mimic the native extracellular matrix and increase the cell guidance [32–34]. Recently, Huang et al. [35] developed an innovative electrospun scaffold combining hydroxyapatite-polyethersulfone with BNC, which promoted nitric oxide release and endothelialization—both crucial for vascular integration in vitro. However, little is known about the performance of NC-based membranes produced via electrospinning or casting as cardiovascular-specific applications, representing a key gap in the current literature.

In this context, the present study investigates the cytocompatibility of two plant-based nanocellulose composite membranes for vascular applications, manufactured via a solvent-casting or electrospinning process. Using HUVECs as a model, we assessed cell proliferation, morphology, the inflammatory response, and monolayer formation in vitro over a 21-day culture period. Special emphasis was placed on understanding how fabrication strategy and resulting membrane physicochemical properties ~~structural differences~~ may modulate cellular viability and metabolic activity. This study also aims to initiate a broader discussion on the potential of plant-based nanocellulose as a sustainable and effective material for cardiovascular graft development.

2. MATERIALS AND METHODS

2.1 Materials

Cellulose nanocrystal (CNC) powder (CelluRodsTM 100P, 150 nm) was purchased from CelluForce Inc. (Canada). Polystyrene (PS, Mw=220,000) was supplied by the State Key Laboratory of Separation Membranes and Membrane Processes (China). The solvent system consisted of a mixture of N,N-dimethylformamide (DMF) and N-methyl-2-pyrrolidone (NMP). DMF (ACS reagent grade, ≥99.8%, Mw=73.09), purchased from Sigma-Aldrich (Germany), and NMP (GC headspace grade, Mw=99.13) was obtained from Fisher Scientific (USA). All chemicals are used as received without further purification.

2.2 Production of NC-based membranes

Nanocellulose membranes were processed via solvent-casting, using 200 µL of NC solution with a concentration of 3.75 $mg.mL^{-1}$ on a 13-mm tissue culture plate (TCP). This method was advantageous for film formation of highly dispersed NC suspensions [36]. The samples were kept for 24 h under ambient conditions (T= 20°C, RH= 40%) to enable complete solvent evaporation.

Electrospun nanocellulose composite membranes were manufactured using polystyrene (PS) particles dispersed in a mixed solvent of N,N-dimethylformamide (DMF) and N-methyl-2-pyrrolidone (NMP) at a volume ratio of 40:60 (v/v) to obtain a solution with a PS concentration of 15 wt%. The PS solution was magnetically stirred at 80 °C for 2 h until complete dissolution was achieved. Subsequently, 0.5 wt% cellulose nanocrystals (CNC) powder was added to the PS solution and sonicated for 10 min using an IKA T18 digital ULTRA-TURRAX homogenizer to remove surface foam. The freshly prepared solution was immediately transferred into four 10 mL syringes, which were mounted onto a syringe pump and connected to feeding tubes. A sheet of silicone-coated paper was affixed to the surface of a 100 mm diameter rotating drum collector. Electrospinning was conducted using a TL-Pro-BM electrospinning apparatus (TONGLI TECH, Shenzhen, China) under room temperature and a relative humidity of 40~50%. The applied voltage was set to 20 kV, the flow rate to 1.0 mL h^{-1}, and the tip-to-collector distance to 15 cm. Upon completion of electrospinning, the product was vacuum-dried for 12 h. The complete manufacturing process is summed up in Figure 1.

2.2 Characterization of NC-based Membranes

2.2.1 Scanning Electron Microscopy (SEM)

The surface characteristics (fibre diameter, pore size) of NC-based membranes were assessed using a HITACHI SEM S-4700. The membrane samples were cut into 5 x 5 mm^2 using a surgical blade, and regions without visible defects were selected for testing. A conductive gold coating was deposited using a Quorum Q150R S ion sputter coater under a current of 10 mA and a vacuum pressure of 5 × 10^{-2} mbar for 90 s. The gold-coated samples were then mounted on stubs with a conductive carbon tape. Surface morphology images were obtained using the secondary electron imaging (SEI) mode. Fibre diameters were randomly measured from different regions of the samples, and the average fibre diameter was calculated to evaluate fibre uniformity and structural distribution.

2.2.2 Dynamic Light Scattering (DLS)

A Litesizer 500 Particle Analyser (Anton Paar) was employed to assess zeta potential, i.e. the charge generated at the interface between a solid and a liquid medium, of NC particles in an aqueous suspension.

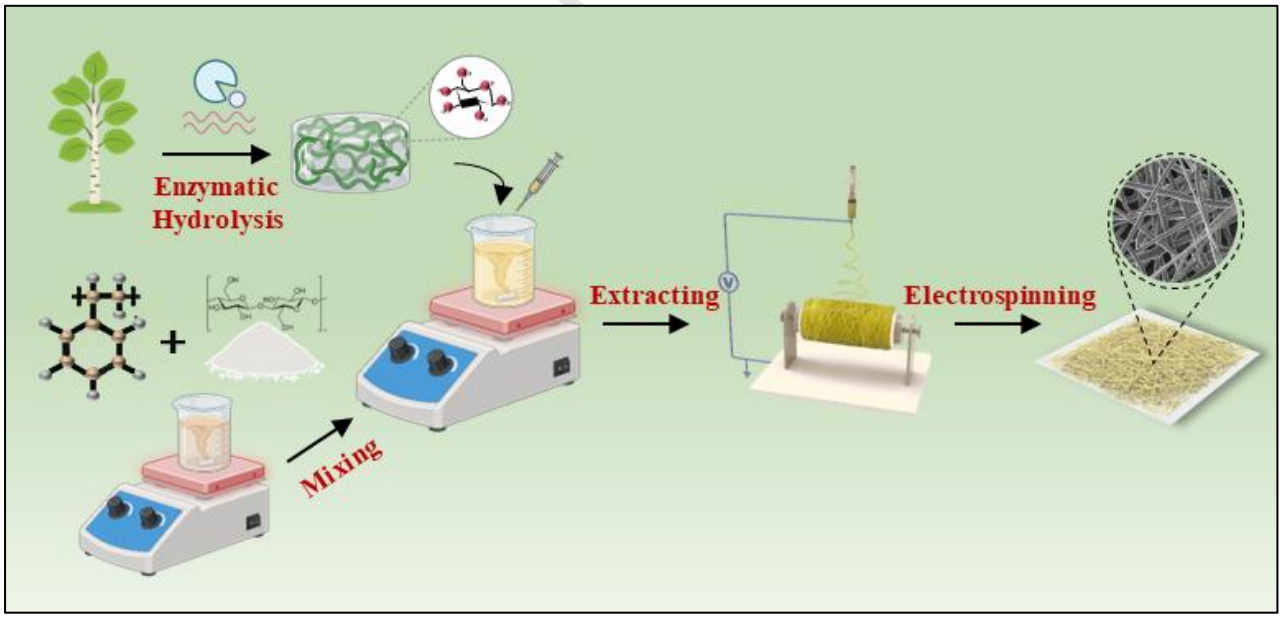

Figure 1: Manufacturing process of electrospun nanocellulose composite membranes.

2.3 Characterization of NC Fibre

2.3.1 Surface roughness and sample thickness

The sample topography of the solvent-cast membrane was qualitatively and quantitively assessed by a Bruker Dimension 3100 AFM. Pictures were taken by using a scan rate of 1 Hz, a scan size of 10 μm

and an amplitude setpoint of 1V. Image processing and roughness measurement were performed with Gwyddion software [37]. The thickness of the solvent-cast membrane was evaluated with a RS-PRO 156H coating thickness tester. Roughness was determined by using a Profilm3D® optical profilometer.

2.3.2 Contact angle measurements

Contact angle measurements were carried out with a customized system in conjugation with Lumenera INFINITY 2-1C Microscope Camera using a 10 µL-volume of distilled water drop.

2.3.3 Fourier-transform infrared spectroscopy (FTIR)

Chemical analysis of NC formulation was performed using a spectrophotometer (IRSpirit, SHIMATZU) at 4000-400cm^{-1}. Prior to testing, all samples were placed overnight in a freeze-dryer (Freezone Labconco) to remove residual water.

2.3.4 Brunauer-Emmett-Teller (BET)

Physical adsorption analyses, including BET, specific surface area, porosity, and pore size distribution, were conducted using an Autosorb iQ series fully automated gas adsorption analyser equipped with ASiQwin-CFR software. Prior to testing, small membrane specimens were degassed under vacuum in a helium atmosphere at 80ºC for 12h. High-purity nitrogen (77 K) was used as the adsorbate, with the relative pressure (P/P0) range set between 10^{-7} and 0.995. The pore distribution was calculated using the BJH (Barrett-Joyner-Halenda) model.

2.4 Biological assays

2.4.1 Cell culture

Primary human umbilical vein endothelial cells (HUVECs) from three different donors were obtained from PromoCell (C-12200) and used to assess the cytocompatibility of the NC-based membranes. Cells were cultured in Endothelial Cell Growth Medium (PromoCell, C-22110) supplemented with Fetal Calf Serum, growth factors (ECGS/H, hVEGF-0.05, HbFGF-0.5, HC-500) and 1% (v/v) penicillin/streptomycin. Cultures were maintained in a humidified incubator (HeraCell 150, ThermoScientific) at 37 °C with 5% CO_2. The passage number was kept between 3 and 10 to ensure phenotypic stability. The culture medium was replaced every two days.

2.4.2 Membrane preparation prior to bio-tests

Both NC-based membranes were immobilised onto a Thermanox coverslip and placed into a 24-well plate. The plates were then sterilized via UV radiation (200-400 nm) for 20 minutes. Afterwards, the samples were kept in sterile conditions under a biological safety hood, washed three times with phosphate-buffered saline (PBS) solution and covered with culture medium overnight. The culture medium was subsequently removed from the wells and HUVEC cells were seeded at 1.10^5 cell/cm^2. To facilitate cellular attachment, the samples were incubated for 4h before the addition of 500 µL of culture medium. The culture medium was collected and stored in -20ºC freezer at day 3, 7, 14 and 21 to perform future proteomics assay.

2.4.3 Analysis of cell proliferation and cell viability was performed via Alamar Blue and Picogreen assays respectively.

Cell proliferation and metabolic activity were assessed using the Alamar Blue assay (DAL1100, Thermo Fisher Scientific). A 10% (v/v) Alamar Blue solution in complete culture medium was added to each well to fully cover the cell-seeded substrates and incubated at 37 °C for 4 hours. Subsequently, 150 µL of supernatant was transferred to a 96-well plate, and absorbance was measured using a Varioskan Flash plate reader (Thermo Fisher Scientific). Measurements were taken at days 1, 3, 7, 14, and 21.

A freeze–thaw cycle was applied to promote cell membrane lysis and release of cytoplasmic double-stranded DNA (dsDNA). The dsDNA content, reflecting total cell number, was quantified using the Quant-iT™ PicoGreen™ dsDNA Assay Kit (P11496, Thermo Fisher Scientific). All assays were performed in biological and technical triplicates.

2.4.4 Immunostaining and confocal analysis

Immunofluorescence triple staining was conducted to evaluate cell morphology and endothelial monolayer formation. Rhodamine Phalloidin (Invitrogen™) was used for F-actin cytoskeleton visualization; Hoechst 33342 – for nuclear staining; and VE-cadherin was detected using a polyclonal primary antibody and an Alexa Fluor 488-conjugated goat anti-rabbit IgG secondary antibody (A-11008, Invitrogen™) to visualize intercellular adherens junctions.

Morphological parameters such as cell area, aspect ratio, and nucleocytoplasmic index were quantitatively analysed using ImageJ, while VE-cadherin staining provided qualitative insight into endothelial monolayer integrity. Imaging was performed via confocal microscopy. All experiments were conducted in biological and technical triplicate.

2.4.5 Protein expression via ELISA and Multiplex ELISA assay

Quantification of endothelial-specific markers was performed using standard ELISA techniques. Expression of platelet endothelial cell adhesion molecule-1 (PECAM-1/CD31) and human vascular endothelial growth factor (hVEGF) was measured using specific ELISA kits (Thermo Fisher Scientific). Additionally, inflammatory cytokine expression was assessed using the LEGENDplex™ Human Inflammation Panel 1 (13-plex, BioLegend), following the manufacturer's protocol.

Samples (minimum 100 µL) were analysed using an Accuri C6 Plus Flow Cytometer (BD Biosciences) under slow fluidics, with a minimum of 4000 events recorded per sample. Gentle agitation was applied every four wells to ensure homogeneity. Data were processed using the LEGENDplex Analysis Software (BioLegend). All experiments were performed in biological and technical triplicates, with measurements taken at days 3, 7, 14, and 21.

2.4.6 Generation of Reactive Oxygen Species (ROS)

Intracellular ROS levels were measured using 2′,7′-dichlorodihydrofluorescein diacetate (DCFH-DA). A fresh 10 µM working solution was prepared from a 10 mM stock in anhydrous DMSO immediately before use. Harvested cells were resuspended in pre-warmed PBS and incubated with the probe at 37 °C for 30 minutes in the dark. After incubation, cells were washed twice with PBS and resuspended in pre-warmed complete medium. Fluorescence was measured using a Cytek Northern Lights 3000 flow cytometer (Cytek Biosciences, USA), and data were analyzed using FlowJo™ software (Version X, BD Biosciences). ROS levels were reported as median fluorescence intensity at days 3, 7, 14, and 21.

2.4.7 Barrier integrity of endothelial monolayer

Endothelial monolayer and barrier integrity was assessed via transepithelial-endothelial electrical resistance (TEER) and permeability assays. Measurements were conducted using an EVOM2

Epithelial Voltohmmeter (World Precision Instruments), providing quantitative data on the integrity of the endothelial monolayer by assessing resistance to electrical current. A Lucifer Yellow CH dye (Thermo Fisher Scientific) was subsequently used to assess molecular permeability across the endothelial barrier. The assay measured the diffusion of the dye into the basal compartment, indirectly indicating tight junction functionality.

2.5 Statistical methods

Statistical significance was determined either using student's t test or one-way analysis of variance (ANOVA) with Tukey's multiple comparisons test. Differences were considered statistically significant at $p < 0.05$. Statistical analyses were performed using Origin (version 8.0.2).

3. RESULTS

3.1 Physicochemical analysis of nanocellulose materials

The physical characteristics of NC-based membranes are displayed in **Error! Reference source not found.**. The zeta potential of -36.4 ± 1.5 mV was obtained for NC suspensions (0.1 wt%) in deionized water, underscoring a stable suspension (> |-30mV|) [38]. Nanocellulose fibres were observable in solvent-cast membranes with a diameter of 21 ± 8 nm. Individual fibres were not observable in electrospun membranes, which were characterised by the presence of a microfibre meshwork with individual fibres measuring 3.3 ± 1.1 µm in diameter (Figure 2).

At higher magnification (Figure 2c), individual fibres were observed to have relatively rough surfaces with multiple pores ranging from 19 to 92 in diameter. In regions of the fibrous network, bead-like structures were also visible (Figure 2d). These features are likely attributed to local variations in concentration and charge density within the electrospinning jet, arising from the polarity difference between PS and CNF, which leads to the formation of characteristic "droplet-filament" morphologies. Solvent-cast membranes possessed a thickness of 4.7 ± 0.5 µm, a water contact angle of 73 ± 6 º, compared to 133 ± 100 µm and 120 ± 4º for electrospun membranes.

Table 1 : Physico-chemical characteristics of solvent-cast and electrospun nanocellulose composite membranes.

Materials	Fibre length (µm)	Fibre diameter (nm)	Aspect Ratio	Membrane Thickness (µm)	Roughness (nm)	Zeta Potential (mV)	Contact angle (ºC)
Solvent-cast membrane	3 ± 1	21 ± 8	150	4.7 ± 0.5	82 ± 43	-29.0 ± 1.0	73 ± 6
Electrospun membrane	-	3350 ± 1100	-	133 ± 97	-	-	120 ± 4

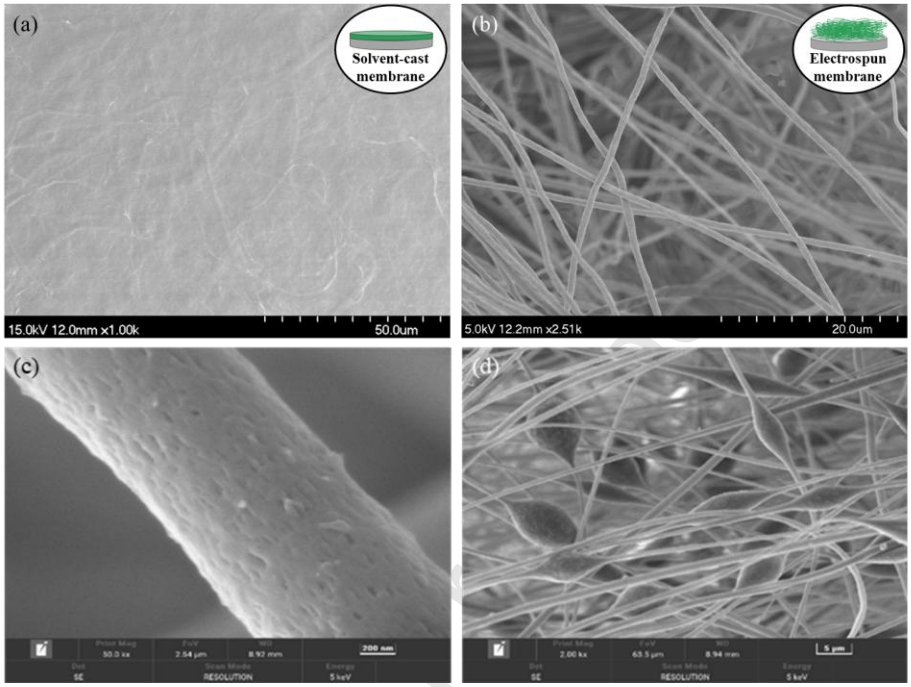

Figure 2: Microscopic images of (a,c) nanocellulose solvent-cast membranes and (b,d) electrospun nanocellulose composite membranes taken at (a,b,d) low and (c) high magnification.

Chemical analysis of both materials is given in Figure 3. FTIR analysis revealed a significant presence of hydroxyl groups as represented by a broad absorption peak at 3400 cm^{-1} in solvent-cast membranes and underscores the interconnection of NC fibres by water molecules. Absorption peaks at 2911 cm^{-1} representing OH- and CH- vibrations and absorption peaks at 1650 to 1600 cm^{-1} represent OH- vibrations of the absorbed water. Peaks at 1314 cm^{-1} and 1162 cm^{-1} indicated the presence of C-O-C and OH in-plane bending vibrations respectively from the polysaccharide rings. The absorption peak observed at 1021 cm^{-1} was attributed to CO- stretching inside the polysaccharide ring (i.e. pyranose). Conclusively the described peaks were highly characteristic of cellulose chemistries [39].

Electrospun composite membranes also exhibited characteristic peaks of nanocellulose at 1024 cm^{-1} (CO- stretching) and 2900 cm^{-1} (OH- and CH- vibrations). Light scattering was promoted by the

heterogenous surfaces [40], which reduced the intensity of the transmitted signal. PS chemistries were affirmed through the presence of peaks at 697 and 749cm-1, related to out-of-plan CH bending, and at 1495 and 1600cm-1, indicating C=C stretching from benzene rings.

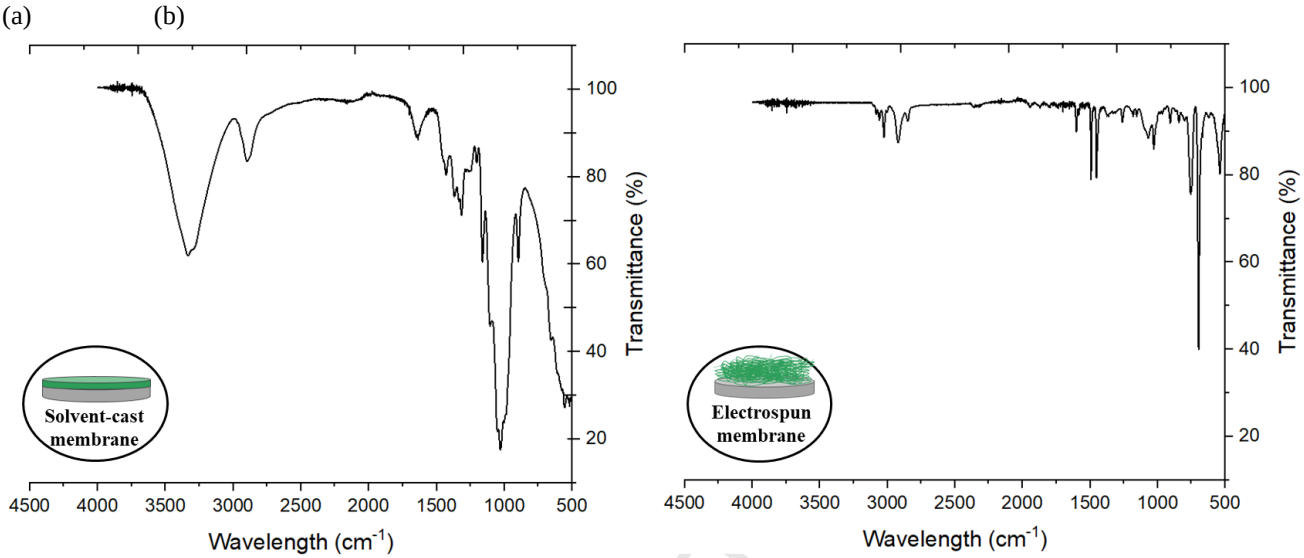

Figure 3: FTIR spectrum of (a) solvent-cast and (b) electrospun nanocellulose composite membranes.

The nitrogen adsorption–desorption isotherm of the solvent-cast membrane (Figure 4a) exhibits a Type II profile, characterized by the absence of a pronounced adsorption uptake at low relative pressures ($P/P_0 < 0.1$), indicating the lack of significant microporosity. Multi-point BET analysis performed within the conventional relative pressure range ($P/P_0 = 0.05–0.30$) did not yield a physically meaningful effective specific surface area, suggesting that the assumptions of the BET model are not satisfied for this dense solvent-cast membrane. In contrast, BJH pore size distribution analysis based on the desorption branch ($P/P_0 = 0.35–0.80$) reveals a limited but measurable mesoporosity, with a total pore volume of approximately 0.154 cm^3/g. The dominant pore radius is centered at 1.56 nm (corresponding to a pore diameter of 3.12 nm), yielding a porosity of approximately 21.0%. These mesopores are attributed to interstitial voids formed between densely packed nanocellulose crystallites or fibrillar aggregates during solvent evaporation and membrane consolidation. Overall, the combined adsorption and pore size analyses demonstrate that the solvent-cast membrane possesses a predominantly compact structure with only minor inter-fibrillar mesoporosity, rather than a highly porous network architecture.

The nitrogen-adsorption-desorption isotherm of the electrospun membrane (Figure 4b) exhibits a typical type IV curve accompanied by a pronounced H3-type hysteresis loop. In the low-pressure region (relative pressure $P/P_o = 10^{-7}–10^{-2}$), the isotherm increased smoothly, indicating the absence of significant micropores (< 2 nm) in the membrane. A steep rise without an evident plateau was observed at a relative pressure range of P/P_o = 0.8–0.9, suggesting that the pore structure of the sample is predominantly composed of slit-like pores formed by the stacking of fibres. The sharp increase in adsorption at this stage results from the physical condensation of nitrogen within macropores or inter-fibre voids.

Based on multipoint fitting of the BET isotherm, software analysis reveals that the electrospun membrane possesses a specific surface area of 244.34 m^2/g, a total pore volume of 9.49 cm^3/g (significantly higher than that of solvent-cast membrane, 0.154 cm^3/g), and a porosity of approximately 92.2%, with an average pore width of about 77.67 nm. These results indicate that the electrospun membrane features a highly porous, fibre-interlaced network dominated by meso- to macropores.

(a) (b)

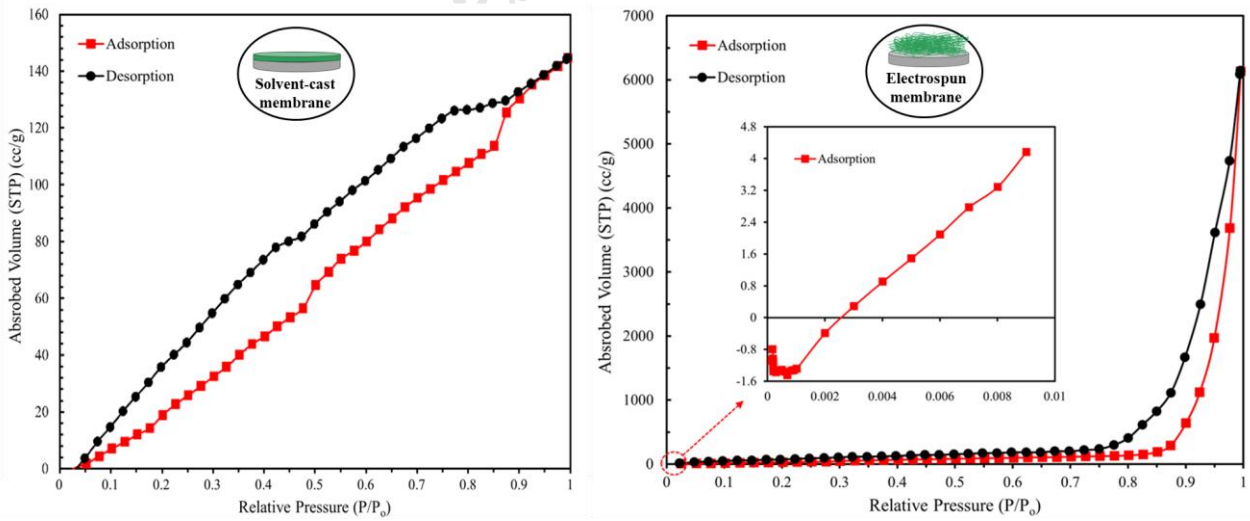

Figure 4: BET adsorption isotherm of (a) solvent-cast NC membrane and (b) electrospun NC composite membranes

3.2 Analysis of Cell/Material interactions in vitro

The metabolic activity of HUVECs cultured on Control and both NC-based membranes was observed to significantly increase over a 21-day culture period as shown in Figure 5a. Cells cultured on solvent-

cast membranes initially exhibit 71.5 ± 19.3% relative fluorescence compared to Control, which increased to 101.2 ± 6.0 % by day 21. This increase in metabolic activity was accompanied by an increase in cell confluency, indicating cytocompatibility. In contrast, electrospun membranes supported a lower metabolic activity, particularly between days 1 and 7, suggesting delayed cell adhesion and subsequent proliferation. This response may be associated with the mesh-like surface of electrospun membranes —high porosity (92.2%) and an average fibre diameter of 3.3 ± 1.1 µm— that may hinder initial cell–material interactions and limit early metabolic engagement.

These trends were corroborated by the quantification of dsDNA synthesis in cells cultured on control and nanocellulose substrates (Figure 5b). HUVECs cultured on both Control and solvent-cast substrates proliferated rapidly, showing a 4.5-fold and 4.2-fold increase in cell number between day 3 and day 7, respectively. In comparison, cell proliferation on electrospun membranes was significantly slower, with only a 3-fold increase in DNA content between day 3 and day 14 in vitro. By day 21, dsDNA levels plateaued across all substrates, reaching $3.0 \pm 0.3\ \mu g \cdot mL^{-1}$ on Control substrates, $2.2 \pm 0.2\ \mu g \cdot mL^{-1}$ on solvent-cast membranes and $2.5 \pm 0.4\ \mu g \cdot mL^{-1}$ on electrospun membranes. These results confirm that although all substrates support HUVEC proliferation, electrospun substrates reduced HUVEC metabolic activity, which is consistent with surface roughness and the substrates porous architecture.

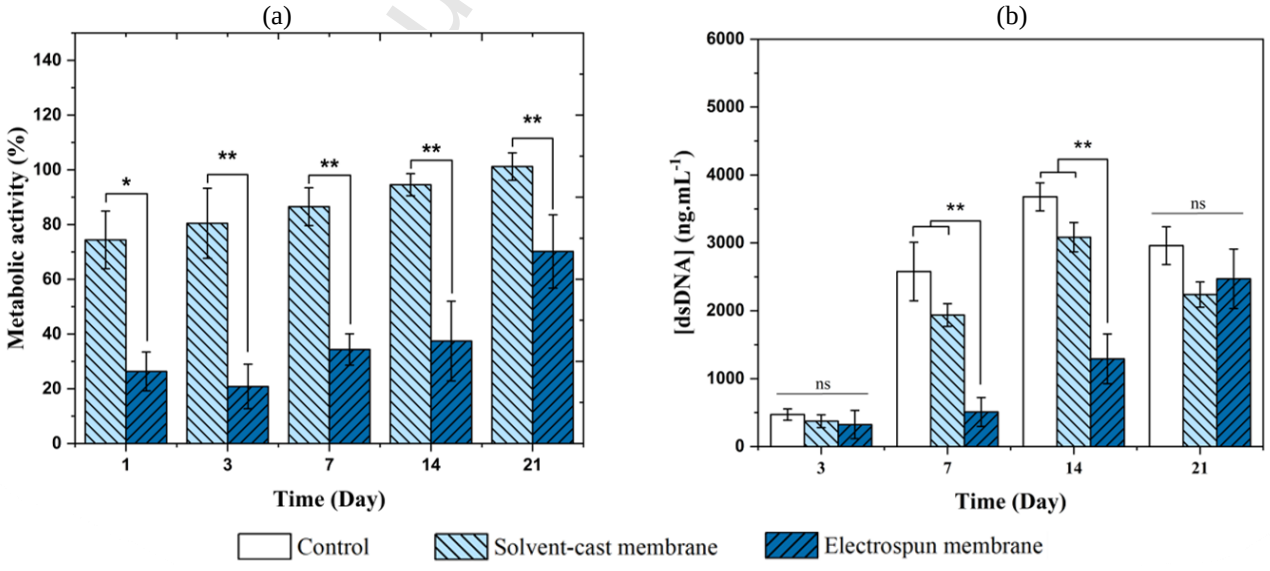

Figure 5: Analysis of (a) cell metabolic activity compared to TCP controls and (b) proliferation of primary endothelial HUVEC cells cultured on TCP controls, solvent-cast membranes and electrospun nanocellulose composite membranes. Data

*are presented as mean ± SD from n = 3 independent experiments. Statistical significance was determined by student's t test and one-way ANOVA with Tukey's post hoc test (*p < 0.05; **p < 0.01; ns = not significant).*

Competent monolayer formation was observed on the Control and NC solvent-cast membranes by day 3, while cells cultured on NC electrospun membranes achieved comparable monolayer coverage by day 21 (Figure 6a). The process of monolayer formation is illustrated in Figure 6b, indicating a significant delay for cells cultured on electrospun membranes at three different timepoints.

To better understand the evolution of cell–material interactions, cell proliferation, and endothelium formation [41], morphometric descriptors—**cell area** and **circularity**—were assessed via immunofluorescent microscopy (Figure 7).

Cell morphometry revealed that at day 1 HUVECs displayed significantly reduced spreading and higher circularity on electrospun membranes compared to solvent-cast membranes, indicative of reduced intracellular tension and cell-matrix adhesion (Figure 7), aligning with the reduced metabolic activity observed at early time points. In contrast, HUVECs on solvent-cast membranes surfaces exhibited increased cell spreading—characteristic of stable attachment and increased intracellular tension from day 1 to day 7 (Figure 7a).

By day 7, HUVECs on electrospun membranes showed a marked increase in cell area and a reduction in circularity (Figure 7b), suggesting enhanced cell spreading and improved adhesion over time. At day 14, both cell area and circularity of HUVECs were comparable between solvent-cast and electrospun membranes. These changes coincide with the observed increase in metabolic activity, confirming the delayed interaction and adhesion of cells on the electrospun membrane surface. Interestingly, the **nucleocytoplasmic ratio** remained similar across all time points, particularly for the electrospun membranes (*Figure S1*, Supplementary Materials). This stability suggests that despite delays in attachment and proliferation, the structural and biological integrity of HUVECs was maintained throughout the culture period, reinforcing the membrane's potential for long-term cytocompatibility.

Flow cytometry analysis of HUVECs stained with H_2DCFDA revealed substrate-dependent differences in intracellular reactive oxygen species (ROS) production, as measured by DCF

fluorescence intensity (Figure 8). On day 3, cells cultured on solvent-cast membranes exhibited significantly lower ROS production relative to cells cultured on both Control (tissue culture plastic), and electrospun membranes ($p < 0.05$). No significant differences were detected among groups on days 7, 14, and 21, with ROS levels decreasing over time across cells cultured on all substrates, indicating progressive cellular adaptation to the material environments and a reduction in oxidative burden at later stages of culture.

To further evaluate the immunological profile and cytocompatibility of NC-based membranes, the secretion of pro- and anti-inflammatory cytokines was assessed in vitro. Figure 9 presents the expression patterns of six key cytokines—IL-6, IL-8, IL-18, IL-23, IFN-α2, and TNF-α—at days 3, 7, 14, and 21. Across all time points, cytokine secretion remained comparable between all experimental and control substrates, with no statistically significant differences detected. Notably, at day 21, cells cultured on electrospun membranes showed consistently lower and more homogenous expression of IL-6, IL-23, IFN-α2, and TNF-α, suggesting a dampened inflammatory response and improved long-term cytocompatibility. Additional cytokines—including IL-1β, IFN-γ, IL-10, IL-12p70, IL-17A, and IL-33— remained below the detection limit across all groups and time points, indicating a generally low pro-inflammatory profile. In contrast, **MCP-1** was the only tested chemokine and was consistently expressed above the detection threshold These data are accessible in the Supplementary Materials section (*Table S1* and *S2*). While this trend points underscored a reduced immune activation, additional factors such as material degradation or altered cellular behaviour should be considered in future investigations.

These findings align with previous reports on the pro-inflammatory responses of HUVECs cultured on nanocellulose materials. For instance, Feil et al. [42] demonstrated that HUVECs cultured on bacterial nanocellulose (Xellunin) showed enhanced responsiveness to pro-inflammatory stimuli compared to those cultured on tissue culture plastic, indicating increased physiological relevance.

3.3 Expression of vascular endothelial growth factor (VEGF)

Figure 10a shows the expression of hVEGF in HUVECs cultured on nanocellulose and control substrates as normalized to dsDNA concentration. Cells cultured on electrospun membranes

demonstrated significantly higher secretion of hVEGF on days 3, 7 and 14, and which decreased by 21. It is assumed that HUVECs cells, facing challenges in adhesion and proliferation at early stages on electrospun membranes, secrete increased hVEGF to support the cell proliferation, differentiation and migration [43].

(a)

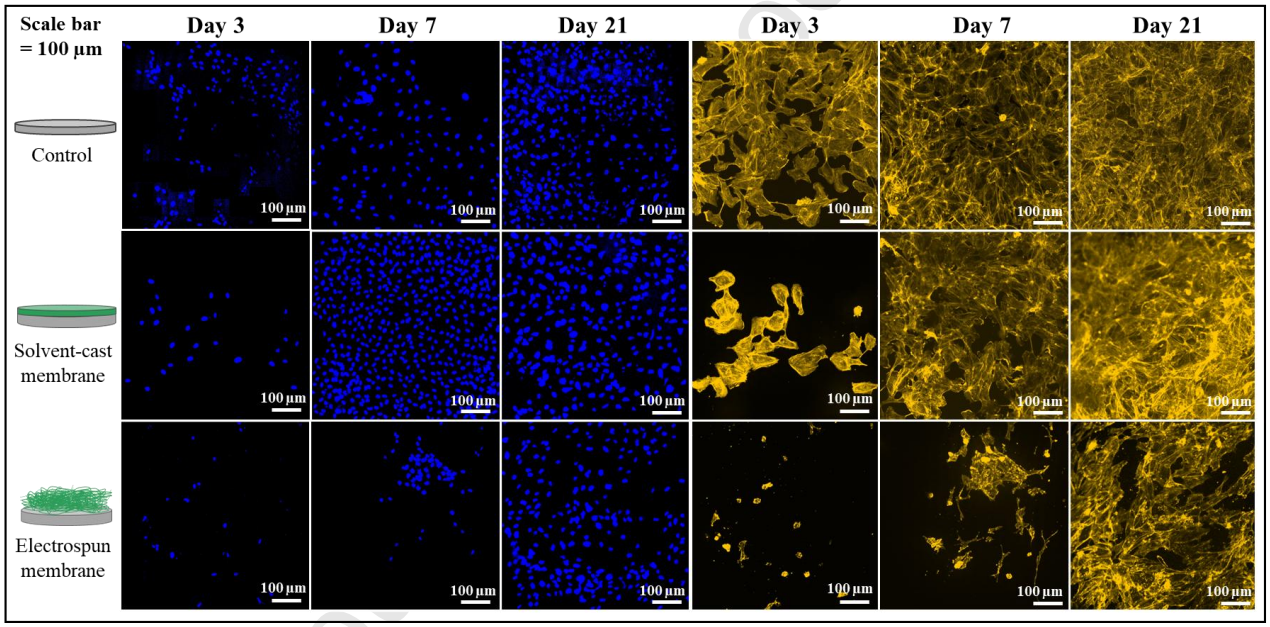

(b)

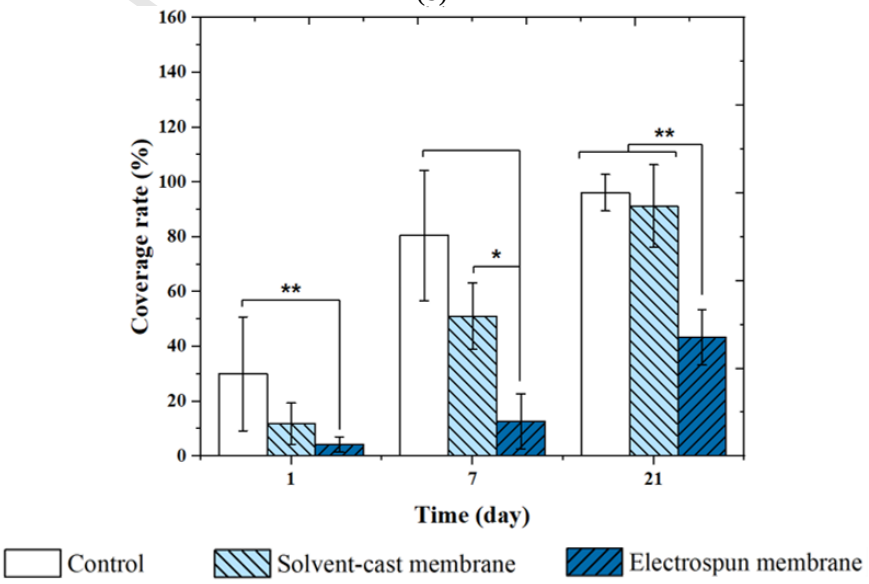

*Figure 6: Immunostaining assay of primary endothelial HUVEC cells cultured on Control (tissue culture plastic), solvent-cast and electrospun nanocellulose composite membranes after 1, 7 and 21 days of culture. (a) Immunofluorescent imaging of nucleus (DAPI) and actin cytoskeleton (Rhodamine Phalloidin). Scale bar = 100 µm. (b) Evolution of coverage rate of HUVEC cells (based on cytoplasmic area) on each material. Data are presented as mean ± SD from n = 3 independent experiments. Statistical significance was determined by one-way ANOVA with Tukey's post hoc test (*p < 0.05; **p < 0.01; ns = not significant).*

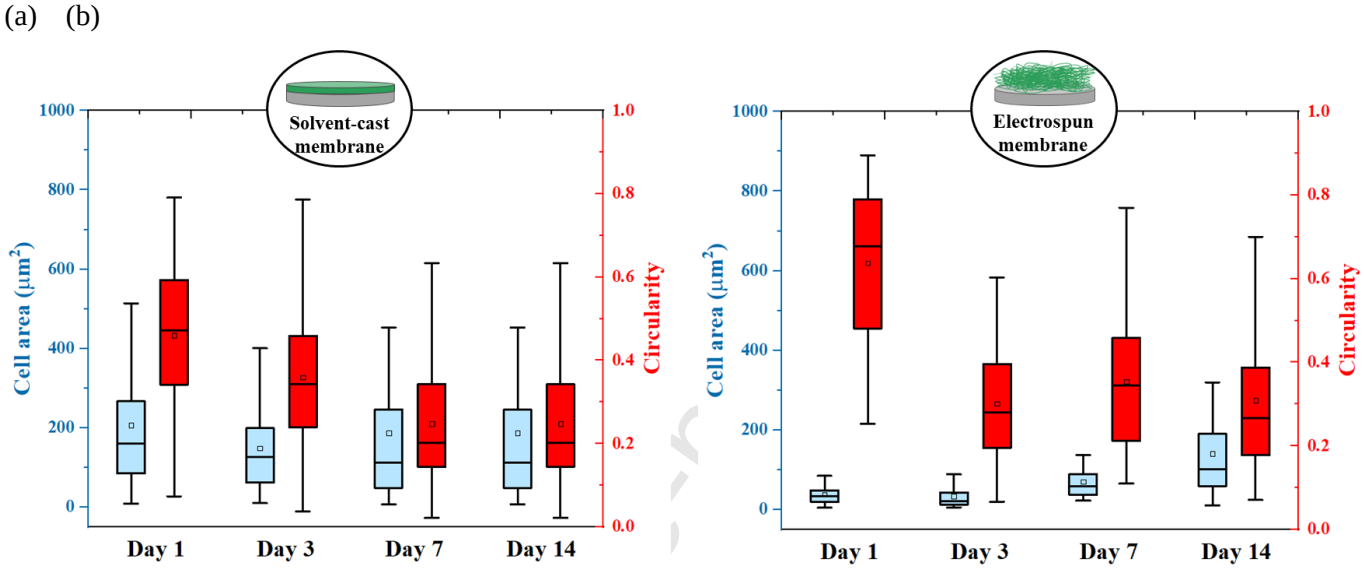

Figure 7: Evolution of morphometric parameters (cell area and circularity) of HUVEC cells (a) on solvent-cast nanocellulose membrane and (b) electrospun membrane from day 1 to day 14. Data are presented as mean ± SD from n = 3 independent experiments.

3.4 Expression of adhesion markers (PECAM-1 and VE-cadherin)

PECAM-1 expression is presented in Figure 10b. While PECAM-1 is primarily know as a transmembrane protein involved in vascular cell adhesion, HUVECs are also capable of secreting a soluble form in the extracellular environment [44]. In this study, PECAM-1 concentration in the supernatant significantly increased between day 7 and day 14, after which it plateaued. Importantly, this trend was consistent across all substrates, with no statistically significant differences observed among the Control, or experimental nanocellulose groups. The presence of the soluble isoform in the culture medium is likely due to alternative splicing mechanisms, as previously reported [44].

To further assess endothelial function and cytocompatibility, the **barrier integrity** of HUVEC monolayers was evaluated, given its central role in regulating nutrient diffusion, intercellular communication, and protection against foreign agents. VE-cadherin, a junctional protein crucial for maintaining endothelial monolayer integrity, was visualized by immunofluorescent imaging at days 3

and 21 (Figure 11). At day 3, HUVECs on the Control surface exhibited strong VE-cadherin expression and 100% confluency, indicative of a mature endothelial monolayer. On solvent-cast membranes, VE-cadherin expression was initially lower, but markedly increased by day 21, highlighting improved cell-cell adhesion and barrier formation over time. In contrast, cells cultured on electrospun membranes

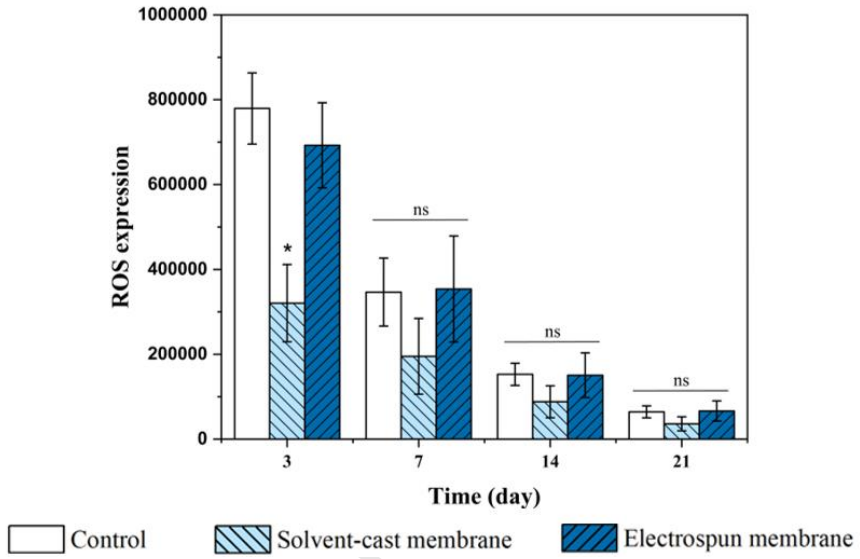

Figure 8: Reactive oxygen species (ROS) levels in human umbilical vein endothelial cells (HUVECs) cultured on Tissue culture plate (white), solvent-cast membranes (light blue), and electrospun membranes (dark blue) at days 3, 7, 14, and 21. Quantification of ROS levels expressed as median fluorescence intensity (MFI).

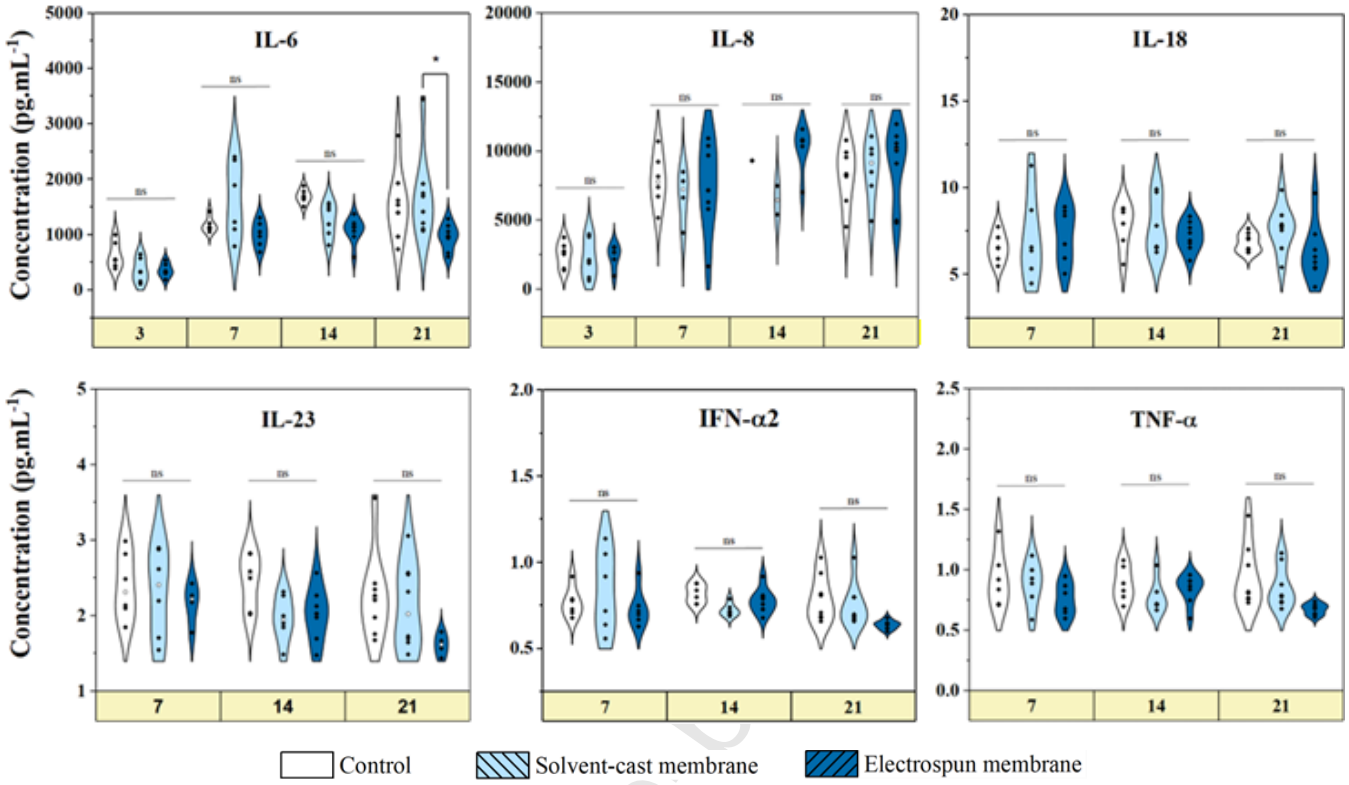

*Figure 9: Expression of proinflammatory cytokines; IL-6, IL-8, IL-18, IL-23, IFN-α2 and TNF-α, by HUVEC cells at days 7, 14 and 21. Data are presented as mean ± SD from n = 3 independent experiments. Statistical significance was determined by one-way ANOVA with Tukey's post hoc test (*p < 0.05; **p < 0.01; ns = not significant).*

(a) (b)

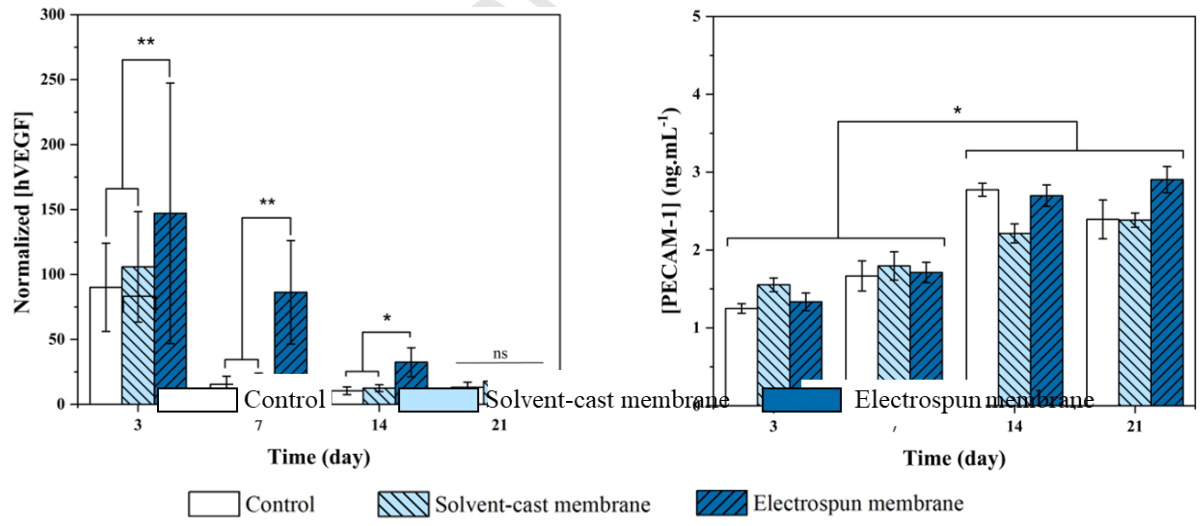

*Figure 10: Extracellular expression of (a) hVEGF proteins and (b) PECAM-1 adhesion proteins by primary endothelial HUVEC cells when interacting with tissue culture plate (Control), solvent-cast and electrospun nanocellulose composite membranes. Data are presented as mean ± SD from n = 3 independent experiments. Statistical significance was determined by one-way ANOVA with Tukey's post hoc test (*p < 0.05; **p < 0.01; ns = not significant).*

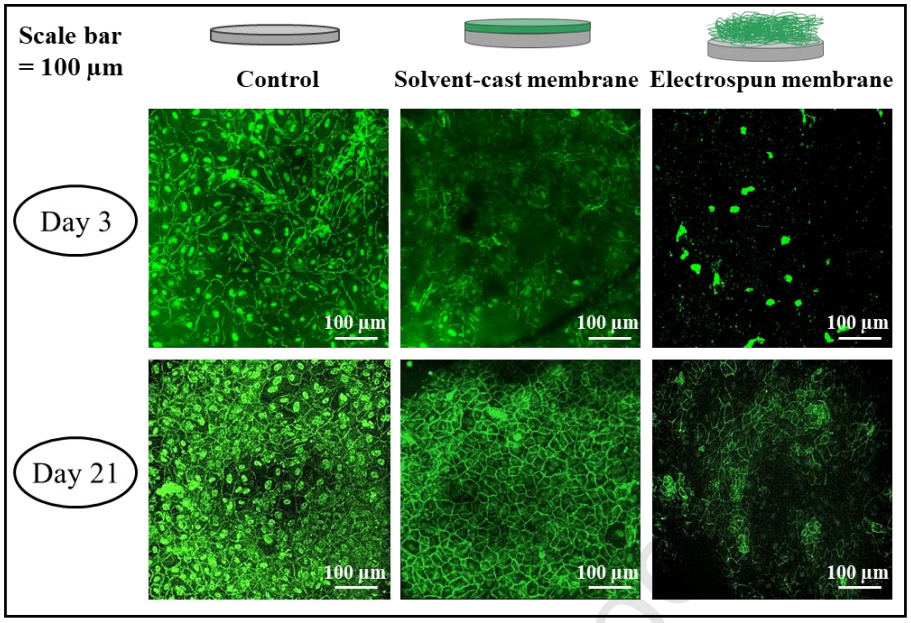

Figure 11: Expression of VE-cadherin adherent junction molecules by primary endothelial HUVEC cells when interacting with tissue culture plate (Control), solvent-cast and electrospun nanocellulose composite membranes Confocal imaging of VE-cadherin expression at the cell-cell junctions at day 3 and day 21. Scale bar = 100 µm.

were not associated with a clear VE-cadherin signal at day 3. By day 14, a slight increase in staining amplitude was observed; however, image interpretation was affected by light interference from the cellulose fibres. This was attributed to spectral overlap between the antibody's emission wavelength (~520 nm) and autofluorescence from the cellulose fibres (~570–585 nm), requiring higher exposure times to visualize cells located both on and beneath the fibre network [41].

To further investigate the barrier function of endothelial monolayers formed on both cast and electrospun substrates, transepithelial electrical resistance (TEER) measurements were performed to quantitatively assess monolayer integrity (*Figure S2* and *S3*, Supplementary Materials). Results confirmed a substantial increase in TEER values on Control and solvent-cast membranes by day 21, consistent with enhanced intercellular connectivity and reduced permeability, as further validated by a Lucifer Yellow-based permeability assay (*Figure S4*, Supplementary Materials). In parallel, VE-cadherin expression was not observed in HUVECs on electrospun membranes until day 21, again, indicating cell proliferation and competent endothelia-like monolayer formation is perturbed on this substrate. However, both TEER and permeability measurements of cells cultured on electrospun membranes yielded unreliable data due to the material's mechanical fragility and high porosity, which disrupted assay reproducibility. These limitations suggest that further optimization of membrane

composition and structural integrity is required to enable robust quantitative assessments in future studies.

4. DISCUSSION

This study investigated the cytocompatibility of two nanocellulose derived membranes —one solvent-cast and one electrospun - using primary human umbilical vein endothelial cells (HUVECs).

An overall positive cellular response was evidenced by a sustained increase in metabolic activity and cell number across both nanocellulose substrates, with proliferation levels comparable to tissue culture plastic by day 21. Notably, the electrospun membrane exhibited delayed early adhesion and proliferation (days 1–7), attributed to its "mesh-like" topography and reduced initial contact points—features commonly associated with electrospun scaffolds. Interestingly, on day 3, HUVECs cultured on the electrospun membrane exhibited higher ROS levels compared with those cultured on the solvent-cast membrane, coinciding with the delayed early proliferation observed on this substrate. This transient increase in ROS may reflect an initial cellular adaptation to the mesh-like architecture of the electrospun scaffold, which provides fewer initial adhesion points and can temporarily alter cytoskeletal organization and mechanotransduction pathways. Importantly, ROS levels decreased over time and became comparable across all substrates, suggesting that the early oxidative response represents a temporary adaptation to the microstructural environment rather than long-term cytotoxicity. The stable cytokine profiles support this assumption.

One of the most notable findings of this study was the delayed endothelial monolayer formation observed on the electrospun nanocellulose composite membranes despite comparable long-term cytocompatibility. This phenomenon is likely attributable to the combined effects of fibre diameter, surface hydrophobicity, and three-dimensional topography. The electrospun membrane exhibited micro-scale fibre diameters (~3.3 μm) and a high contact angle (~120°), both of which are known to reduce initial focal adhesion formation and limit integrin-mediated signalling during early cell–material interaction, leading to a delayed cytoskeletal remodelling and intercellular communication. In contrast, the nanoscale fibrillar structure and higher hydrophilicity of the solvent-cast membrane

provided a more continuous adhesive interface, facilitating rapid cell spreading and junction establishment. These observations suggest that early endothelialization on nanocellulose substrates is not solely governed by chemical composition but is strongly influenced by micro- and nanoscale architectural cues. Indeed, the highly porous architecture (≈92% porosity) and interconnected fibre network may promote cell infiltration and three-dimensional tissue integration, features that are potentially advantageous for in vivo vascular graft applications [45–47]. In physiological settings, complete endothelial coverage is often accompanied by transmural cell migration and extracellular matrix remodeling [46,47]. Therefore, the electrospun configuration may offer structural benefits that are not fully captured in static in vitro monolayer assays. This distinction highlights the need to interpret delayed in vitro endothelialization cautiously, particularly for biomaterials intended for dynamic vascular environments.

These findings align with previous reports on the ability of nanocellulose to support endothelial function. Feil et al. [42] demonstrated that HUVECs cultured on bacterial nanocellulose (Xellulin) re-expressed CD34—a stem/progenitor cell marker typically lost in standard culture—suggesting that nanocellulose may help maintain a more physiologically relevant endothelial phenotype. Furthermore, the inherent porosity of nanocellulose scaffolds supports angiogenesis and facilitates endothelial migration—critical factors in vascular graft integration [46,47]. Importantly, endothelial behaviour is highly influenced by initial cell seeding density. Higher seeding densities may enhance endothelialization on complex substrates like the electrospun membrane, potentially accelerating monolayer formation [48]. This parameter warrants further investigation and optimization in future studies.

To further improve cellular outcomes, structural refinement of the electrospun nanocellulose composite membranes through high-rpm electrospinning might further promote endothelial function in vitro. Fibre alignment has been shown to modulate hydrophilicity, cytoskeletal organization, and directional cell growth. Whited and Rylander [49], for example, reported improved HUVEC alignment and F-actin organization on aligned polycaprolactone (PCL) scaffolds. Additionally, fibre diameter is an important consideration, as smaller fibre diameters ($d < 2\mu m$) have been associated

with increased apoptosis in endothelial cells [50]. Surface functionalization is another promising approach. Surface coating of nanocellulose scaffolds with extracellular matrix proteins (e.g., collagen or laminin) has also been shown to enhance endothelial adhesion and maturation [51]. Likewise, chemical modifications—such as amination or sulfonation—can introduce charged functional groups that improve hydrophilicity and modulate cellular responses [52].

Nanocellulose-based biomaterials are emerging as sustainable, tunable alternatives for cardiovascular implants [24,53,54]. While previous studies have explored the immunomodulatory effects of modified nanocellulose on various human cell types (e.g., lung epithelial cells) [55], the cellular mechanisms governing endothelial proliferation, differentiation, and barrier formation on electrospun nanocellulose-based membranes remain underexplored.

To the authors' knowledge, this is the first report evaluating in a comparative and exploratory in vitro context the cytocompatibility of electrospun nanocellulose composite membranes with primary human endothelial cells. The results demonstrate the material's ability to support endothelial attachment, proliferation, and intercellular junction formation, underscoring its potential for vascular tissue engineering platform materials. These findings contribute to the foundation for developing biodegradable, sustainable vascular grafts and highlight electrospun nanocellulose composite membranes as promising candidates for next-generation cardiovascular devices. However, several limitations of the present study should be acknowledged. First, the electrospun membrane incorporated polystyrene as a carrier polymer, introducing compositional differences that may confound purely structure-driven interactions. Second, barrier integrity measurements on electrospun membranes were limited by mechanical fragility and high porosity, preventing robust quantitative comparisons. Third, the use of static culture conditions does not replicate the shear stress and hemodynamic forces that critically regulate the shear stress and hemodynamic forces that critically regulate endothelial maturation in vivo [56,57]. Future studies should therefore focus on refining membrane mechanical stability, exploring fibre alignment strategies [49], and evaluating endothelial responses under physiological flow conditions. Additionally, incorporating bioactive surface

functionalization or extracellular matrix coatings [51,52] may help overcome early adhesion limitations while preserving the structural advantages of electrospun architectures.

5. CONCLUSION

In this study, an electrospun nanocellulose composite membrane was comparatively evaluated to a solvent-cast nanocellulose membrane for their in vitro cytocompatibility with primary human umbilical vein endothelial cells (HUVECs). Both membrane systems supported endothelial cell attachment and proliferation without including significant proinflammatory responses, and the observed decrease in reactive oxygen species over time indicated a low oxidative stress environment during prolonged culture.

While solvent-cast membranes facilitated earlier endothelial maturation, as reflected by more consistent PECAM-1 and VE-cadherin expression and the formation of a confluent monolayer, electrospun membranes exhibited delayed endothelial coverage and incomplete monolayer formation within the same culture period. These observations suggest that differences in fabrication strategy and the resulting surface architecture influence endothelial behaviour under the tested conditions. Taken together, these findings highlight plant-derived nanocellulose as a biocompatible and environmentally sustainable material platform for endothelial cell-material interaction studies. Although further optimization of electrospun nanocellulose composite membranes - such as adjusting fibre organization, diameter, and surface chemistry - will be necessary to improve endothelial integration, the present work provides a comparative and explanatory foundation for future investigations of nanocellulose composite biomaterials in vascular-related biomedical applications.

ACKNOWLEDGEMENTS

This current work is part of the CellMembrane Project funded by the European Innovation Council (EIC) Pathfinder (Grant Agreement No: 101130895). This paper has also been funded through Science Foundation Ireland (SFI) and the European Regional Development Fund (grant number 13/RC/2073). The authors acknowledge the facilities and scientific and technical assistance of the Centre for Microscopy & Imaging at the University of Galway (www.imaging.nuigalway.ie). They

thank Dr Kudina and Mr Doulgkeroglou, lab managers in the Research Ireland Centre for Medical Devices as well as Dr. Shirley of the Flow Cytometry core facility and Dr. Enda O'Connell of the Genomics and Screening core facility in the Technology Services Directorate (University of Galway) for support and assistance in this work. Finally, the authors would like to thank the different partners of the CellMembrane project (Smart Reactors, Cellink, University of Tubingen and NOVA University of Lisboa) for their support and collaboration.

REFERENCES

[1] K. Hu, Y. Li, Z. Ke, H. Yang, C. Lu, Y. Li, Y. Guo, History, progress and future challenges of artificial blood vessels: a narrative review, Biomater. Transl. 81–98 (2022). https://doi.org/https://doi.org/10.12336/biomatertransl.2022.01.008.

[2] Q. Li, X. Ding, C. Chen, K. Zhang, R. Dong, An overview of small diameter vascular grafts: from materials to fabrication, Mater. Adv. 6 (2025) 6221–6242. https://doi.org/10.1039/D5MA00663E.

[3] R. Zizhou, X. Wang, S. Houshyar, Review of Polymeric Biomimetic Small-Diameter Vascular Grafts to Tackle Intimal Hyperplasia, ACS Omega 7 (2022) 22125–22148. https://doi.org/10.1021/acsomega.2c01740.

[4] M.-X. Li, Q.-Q. Wei, H.-L. Mo, Y. Ren, W. Zhang, H.-J. Lu, Y.K. Joung, Challenges and advances in materials and fabrication technologies of small-diameter vascular grafts, Biomater. Res. 27 (2023) 58. https://doi.org/10.1186/s40824-023-00399-2.

[5] H. Ding, X. Hou, Z. Gao, Y. Guo, B. Liao, J. Wan, Challenges and Strategies for Endothelializing Decellularized Small-Diameter Tissue-Engineered Vessel Grafts, Adv. Healthc. Mater. 13 (2024) 2304432. https://doi.org/10.1002/adhm.202304432.

[6] S. Fang, D.G. Ellman, D.C. Andersen, Review: Tissue Engineering of Small-Diameter Vascular Grafts and Their In Vivo Evaluation in Large Animals and Humans, Cells 10 (2021) 713. https://doi.org/10.3390/cells10030713.

[7] M.A. Rodríguez-Soto, C.A. Polanía-Sandoval, A.M. Aragón-Rivera, D. Buitrago, M. Ayala-Velásquez, A. Velandia-Sánchez, G. Peralta Peluffo, J.C. Cruz, C. Muñoz Camargo, J. Camacho-Mackenzie, J.G. Barrera-Carvajal, J.C. Briceño, Small Diameter Cell-Free Tissue-Engineered Vascular Grafts: Biomaterials and Manufacture Techniques to Reach Suitable Mechanical Properties, Polymers 14 (2022) 3440. https://doi.org/10.3390/polym14173440.

[8] D. Hernandez-Sanchez, M. Comtois-Bona, M. Muñoz, M. Ruel, E.J. Suuronen, E.I. Alarcon, Manufacturing and validation of small-diameter vascular grafts: A mini review, iScience 27 (2024) 109845. https://doi.org/10.1016/j.isci.2024.109845.

[9] A. Dufresne, Nanocellulose: a new ageless bionanomaterial, Mater. Today 16 (2013) 220–227. https://doi.org/10.1016/j.mattod.2013.06.004.

[10] J.T. McNamara, J.L.W. Morgan, J. Zimmer, A Molecular Description of Cellulose Biosynthesis, Annu. Rev. Biochem. 84 (2015) 895–921. https://doi.org/10.1146/annurev-biochem-060614-033930.

[11] B. Azimi, S. Sepahvand, S. Ismaeilimoghadam, H. Kargarzadeh, A. Ashori, M. Jonoobi, S. Danti, Application of Cellulose-Based Materials as Water Purification Filters; A State-of-the-Art Review, J. Polym. Environ. 32 (2024) 345–366. https://doi.org/10.1007/s10924-023-02989-6.

[12] C.P. Teng, M.Y. Tan, J.P.W. Toh, Q.F. Lim, X. Wang, D. Ponsford, E.M.J. Lin, W. Thitsartarn, S.Y. Tee, Advances in Cellulose-Based Composites for Energy Applications, Materials 16 (2023) 3856. https://doi.org/10.3390/ma16103856.
[13] W. Tu, S. Wang, Q. Deng, D. Li, Y. Zhang, Q. Wang, H. Jiang, Review on nanocellulose composites and CNFs assembled microfiber toward automotive applications, Nanotechnol. Rev. 13 (2024) 20240006. https://doi.org/10.1515/ntrev-2024-0006.
[14] S. Sozcu, M. Venkataraman, J. Wiener, B. Tomkova, J. Militky, A. Mahmood, Incorporation of Cellulose-Based Aerogels into Textile Structures, Materials 17 (2023) 27. https://doi.org/10.3390/ma17010027.
[15] F.V. Ferreira, A.G. Souza, R. Ajdary, L.P. De Souza, J.H. Lopes, D.S. Correa, G. Siqueira, H.S. Barud, D.D.S. Rosa, L.H.C. Mattoso, O.J. Rojas, Nanocellulose-based porous materials: Regulation and pathway to commercialization in regenerative medicine, Bioact. Mater. 29 (2023) 151–176. https://doi.org/10.1016/j.bioactmat.2023.06.020.
[16] D. Liu, Q. Meng, J. Hu, Bacterial Nanocellulose Hydrogel: A Promising Alternative Material for the Fabrication of Engineered Vascular Grafts, Polymers 15 (2023) 3812. https://doi.org/10.3390/polym15183812.
[17] L. Bacakova, J. Pajorova, M. Bacakova, A. Skogberg, P. Kallio, K. Kolarova, V. Svorcik, Versatile Application of Nanocellulose: From Industry to Skin Tissue Engineering and Wound Healing, Nanomaterials 9 (2019) 164. https://doi.org/10.3390/nano9020164.
[18] Q. Wang, Q. Yao, J. Liu, J. Sun, Q. Zhu, H. Chen, Processing nanocellulose to bulk materials: a review, Cellulose 26 (2019) 7585–7617. https://doi.org/10.1007/s10570-019-02642-3.
[19] Y. Lu, P. Tao, N. Zhang, S. Nie, Preparation and thermal stability evaluation of cellulose nanofibrils from bagasse pulp with differing hemicelluloses contents, Carbohydr. Polym. 245 (2020) 116463. https://doi.org/10.1016/j.carbpol.2020.116463.
[20] Q. Tarrés, N.V. Ehman, M.E. Vallejos, M.C. Area, M. Delgado-Aguilar, P. Mutjé, Lignocellulosic nanofibers from triticale straw: The influence of hemicelluloses and lignin in their production and properties, Carbohydr. Polym. 163 (2017) 20–27. https://doi.org/10.1016/j.carbpol.2017.01.017.
[21] L. Bao, J. Tang, F.F. Hong, X. Lu, L. Chen, Physicochemical Properties and In Vitro Biocompatibility of Three Bacterial Nanocellulose Conduits for Blood Vessel Applications, Carbohydr. Polym. 239 (2020) 116246. https://doi.org/10.1016/j.carbpol.2020.116246.
[22] M.S. Hasanin, Cellulose-Based Biomaterials: Chemistry and Biomedical Applications, Starch - Stärke 74 (2022) 2200060. https://doi.org/10.1002/star.202200060.
[23] S. Naz, J.S. Ali, M. Zia, Nanocellulose isolation characterization and applications: a journey from non-remedial to biomedical claims, Bio-Des. Manuf. 2 (2019) 187–212. https://doi.org/10.1007/s42242-019-00049-4.
[24] L. Lin, L. Chen, G. Chen, C. Lu, F.F. Hong, Effects of heterogeneous surface characteristics on hemocompatibility and cytocompatibility of bacterial nanocellulose, Carbohydr. Polym. 335 (2024) 122063. https://doi.org/10.1016/j.carbpol.2024.122063.
[25] M. Kaczmarek, A.M. Białkowska, Enzymatic functionalization of bacterial nanocellulose: current approaches and future prospects, J. Nanobiotechnology 23 (2025) 82. https://doi.org/10.1186/s12951-025-03163-x.
[26] A. Bernier, T. Tobias, H. Nguyen, S. Kumar, B. Tuga, Y. Imtiaz, C.W. Smith, R. Sunasee, K. Ckless, Vascular and Blood Compatibility of Engineered Cationic Cellulose Nanocrystals in Cell-Based Assays, Nanomaterials 11 (2021) 2072. https://doi.org/10.3390/nano11082072.
[27] X. Wang, C.H. Chang, J. Jiang, Q. Liu, Y. Liao, J. Lu, L. Li, X. Liu, J. Kim, A. Ahmed, A.E. Nel, T. Xia, The Crystallinity and Aspect Ratio of Cellulose Nanomaterials Determine Their Pro-Inflammatory and Immune Adjuvant Effects In Vitro and In Vivo, Small 15 (2019) 1901642. https://doi.org/10.1002/smll.201901642.

[28] F. Blank, B.M. Rothen-Rutishauser, S. Schurch, P. Gehr, An Optimized *In Vitro* Model of the Respiratory Tract Wall to Study Particle Cell Interactions, J. Aerosol Med. 19 (2006) 392–405. https://doi.org/10.1089/jam.2006.19.392.
[29] C. Endes, O. Schmid, C. Kinnear, S. Mueller, S. Camarero-Espinosa, D. Vanhecke, E.J. Foster, A. Petri-Fink, B. Rothen-Rutishauser, C. Weder, M.J. Clift, An in vitro testing strategy towards mimicking the inhalation of high aspect ratio nanoparticles, Part. Fibre Toxicol. 11 (2014) 40. https://doi.org/10.1186/s12989-014-0040-x.
[30] C. Endes, S. Mueller, C. Kinnear, D. Vanhecke, E.J. Foster, A. Petri-Fink, C. Weder, M.J.D. Clift, B. Rothen-Rutishauser, Fate of Cellulose Nanocrystal Aerosols Deposited on the Lung Cell Surface In Vitro, Biomacromolecules 16 (2015) 1267–1275. https://doi.org/10.1021/acs.biomac.5b00055.
[31] J. Catalán, M. Ilves, H. Järventaus, K. Hannukainen, E. Kontturi, E. Vanhala, H. Alenius, K.M. Savolainen, H. Norppa, Genotoxic and immunotoxic effects of cellulose nanocrystals in vitro, Environ. Mol. Mutagen. 56 (2015) 171–182. https://doi.org/10.1002/em.21913.
[32] P. Cai, Y. Ding, C. Wang, J. Wu, M.L. Hart, B. Rolauffs, X. Mo, B. Sun, Advancing biomimetic bone Scaffolds: From electrospun 2D membranes to functional 3D nanofiber constructs, Biomed. Technol. 11 (2025) 100099. https://doi.org/10.1016/j.bmt.2025.100099.
[33] Y. Xu, Q. Saiding, X. Zhou, J. Wang, W. Cui, X. Chen, Electrospun fiber-based immune engineering in regenerative medicine, Smart Med. 3 (2024) e20230034. https://doi.org/10.1002/SMMD.20230034.
[34] Y. Song, Q. Hu, S. Liu, G. Yao, H. Zhang, Electrospinning drug-loaded polycaprolactone/polycaprolactone-gelatin multi-functional bilayer nanofibers composite scaffold for postoperative wound healing of cutaneous squamous cell carcinoma, Biomed. Technol. 8 (2024) 65–80. https://doi.org/10.1016/j.bmt.2024.10.001.
[35] Z. Huang, W. Yao, Z. Yang, H. Luo, Y. Wan, Q. Zhang, Incorporating hydroxyapatite and micro-nano-fibrous structure into cardiovascular scaffold for improved hemocompatibility and endothelialization, J. Nanoparticle Res. 27 (2025) 97. https://doi.org/10.1007/s11051-025-06294-2.
[36] K. Zhao, X. Yu, R. Li, A. Amassian, Y. Han, Solvent-dependent self-assembly and ordering in slow-drying drop-cast conjugated polymer films, J. Mater. Chem. C 3 (2015) 9842–9848. https://doi.org/10.1039/C5TC02415C.
[37] D. Nečas, P. Klapetek, Gwyddion: an open-source software for SPM data analysis, Open Phys. 10 (2012) 181–188. https://doi.org/10.2478/s11534-011-0096-2.
[38] B.P. Singh, R. Menchavez, C. Takai, M. Fuji, M. Takahashi, Stability of dispersions of colloidal alumina particles in aqueous suspensions, J. Colloid Interface Sci. 291 (2005) 181–186. https://doi.org/10.1016/j.jcis.2005.04.091.
[39] W.T. Wulandari, A. Rochliadi, I.M. Arcana, Nanocellulose prepared by acid hydrolysis of isolated cellulose from sugarcane bagasse, IOP Conf. Ser. Mater. Sci. Eng. 107 (2016) 012045. https://doi.org/10.1088/1757-899X/107/1/012045.
[40] P.L. Almeida, S. Kundu, J.P. Borges, M.H. Godinho, J.L. Figueirinhas, Electro-optical light scattering shutter using electrospun cellulose-based nano- and microfibers, Appl. Phys. Lett. 95 (2009) 043501. https://doi.org/10.1063/1.3186640.
[41] Q. Ding, W. Han, X. Li, Y. Jiang, C. Zhao, New insights into the autofluorescence properties of cellulose/nanocellulose, Sci. Rep. 10 (2020) 21387. https://doi.org/10.1038/s41598-020-78480-2.
[42] G. Feil, R. Horres, J. Schulte, A.F. Mack, S. Petzoldt, C. Arnold, C. Meng, L. Jost, J. Boxleitner, N. Kiessling-Wolf, E. Serbest, D. Helm, B. Kuster, I. Hartmann, T. Korff, H. Hahne, Bacterial Cellulose Shifts Transcriptome and Proteome of Cultured Endothelial Cells Towards Native Differentiation, Mol. Cell. Proteomics 16 (2017) 1563–1577. https://doi.org/10.1074/mcp.RA117.000001.
[43] A. Yoshida, B. Anand-apte, B.R. Zetter, Differential Endothelial Migration and Proliferation to Basic Fibroblast Growth Factor and Vascular Endothelial Growth Factor, Growth Factors 13 (1996) 57–64. https://doi.org/10.3109/08977199609034566.

[44] A. Goldberger, K.A. Middleton, J.A. Oliver, C. Paddock, H.C. Yan, H.M. DeLisser, S.M. Albelda, P.J. Newman, Biosynthesis and processing of the cell adhesion molecule PECAM-1 includes production of a soluble form., J. Biol. Chem. 269 (1994) 17183–17191. https://doi.org/10.1016/S0021-9258(17)32538-3.
[45] G.N. Arjun, P. Ramesh, Structural characterization, mechanical properties, and *in vitro* cytocompatibility evaluation of fibrous polycarbonate urethane membranes for biomedical applications, J. Biomed. Mater. Res. A 100A (2012) 3042–3050. https://doi.org/10.1002/jbm.a.34255.
[46] D. Jerka, K. Bonowicz, K. Piekarska, S. Gokyer, U.S. Derici, O.A. Hindy, B.B. Altunay, I. Yazgan, K. Steinbrink, K. Kleszczyński, P. Yilgor, M. Gagat, Unraveling Endothelial Cell Migration: Insights into Fundamental Forces, Inflammation, Biomaterial Applications, and Tissue Regeneration Strategies, ACS Appl. Bio Mater. 7 (2024) 2054–2069. https://doi.org/10.1021/acsabm.3c01227.
[47] S. Kratzer, A. Arkudas, M. Himmler, D.W. Schubert, D. Schneidereit, J. Bauer, O. Friedrich, R.E. Horch, A. Cai, Vascularization of Poly-ε-Caprolactone-Collagen I-Nanofibers with or without Sacrificial Fibers in the Neurotized Arteriovenous Loop Model, Cells 11 (2022) 3774. https://doi.org/10.3390/cells11233774.
[48] B.C. Heng, P.P. Bezerra, P.R. Preiser, S.K. Alex Law, Y. Xia, F. Boey, S.S. Venkatraman, Effect of cell-seeding density on the proliferation and gene expression profile of human umbilical vein endothelial cells within ex vivo culture, Cytotherapy 13 (2011) 606–617. https://doi.org/10.3109/14653249.2010.542455.
[49] B.M. Whited, M.N. Rylander, The influence of electrospun scaffold topography on endothelial cell morphology, alignment, and adhesion in response to fluid flow, Biotechnol. Bioeng. 111 (2014) 184–195. https://doi.org/10.1002/bit.24995.
[50] J.A. Reid, A. McDonald, A. Callanan, Modulating electrospun polycaprolactone scaffold morphology and composition to alter endothelial cell proliferation and angiogenic gene response, PLOS ONE 15 (2020) e0240332. https://doi.org/10.1371/journal.pone.0240332.
[51] A.N. Shishparenok, V.V. Furman, N.V. Dobryakova, D.D. Zhdanov, Protein Immobilization on Bacterial Cellulose for Biomedical Application, Polymers 16 (2024) 2468. https://doi.org/10.3390/polym16172468.
[52] S. Tortorella, V. Vetri Buratti, M. Maturi, L. Sambri, M. Comes Franchini, E. Locatelli, Surface-Modified Nanocellulose for Application in Biomedical Engineering and Nanomedicine: A Review, Int. J. Nanomedicine Volume 15 (2020) 9909–9937. https://doi.org/10.2147/IJN.S266103.
[53] F.K. Andrade, R. Costa, L. Domingues, R. Soares, M. Gama, Improving bacterial cellulose for blood vessel replacement: Functionalization with a chimeric protein containing a cellulose-binding module and an adhesion peptide, Acta Biomater. 6 (2010) 4034–4041. https://doi.org/10.1016/j.actbio.2010.04.023.
[54] L. Bao, F.F. Hong, G. Li, G. Hu, L. Chen, Improved Performance of Bacterial Nanocellulose Conduits by the Introduction of Silk Fibroin Nanoparticles and Heparin for Small-Caliber Vascular Graft Applications, Biomacromolecules 22 (2021) 353–364. https://doi.org/10.1021/acs.biomac.0c01211.
[55] V.R. Lopes, C. Sanchez-Martinez, M. Strømme, N. Ferraz, In vitro biological responses to nanofibrillated cellulose by human dermal, lung and immune cells: surface chemistry aspect, Part. Fibre Toxicol. 14 (2017) 1. https://doi.org/10.1186/s12989-016-0182-0.
[56] J.-J. Chiu, S. Chien, Effects of Disturbed Flow on Vascular Endothelium: Pathophysiological Basis and Clinical Perspectives, Physiol. Rev. 91 (2011) 327–387. https://doi.org/10.1152/physrev.00047.2009.
[57] P.F. Davies, Flow-mediated endothelial mechanotransduction, Physiol. Rev. 75 (1995) 519–560. https://doi.org/10.1152/physrev.1995.75.3.519.

Declaration of Interest Statement

☒ The authors declare that they have no known competing financial interests or personal relationships that could have appeared to influence the work reported in this paper.

☐ The author is an Editorial Board Member/Editor-in-Chief/Associate Editor/Guest Editor for this journal and was not involved in the editorial review or the decision to publish this article.

☐ The authors declare the following financial interests/personal relationships which may be considered as potential competing interests:

Statement of Significance

This study introduces electrospun nanocellulose composite membranes as a sustainable alternative to synthetic polymers commonly used in vascular grafts. Unlike traditional petrochemical-based materials, nanocellulose is renewable, eco-friendly, and demonstrates excellent compatibility with human endothelial cells. We provide a systematic evaluation of cell viability, proliferation, and endothelial barrier function on nanocellulose membranes compared with conventional culture systems. The novelty lies in combining advanced electrospinning technology with natural cellulose nanocrystals (CNC) to create a membrane that is both biologically supportive and environmentally responsible. This work advances the understanding of nanocellulose in cardiovascular applications and highlights its potential to inspire greener, safer biomaterials for tissue engineering and regenerative medicine.

Graphical abstract

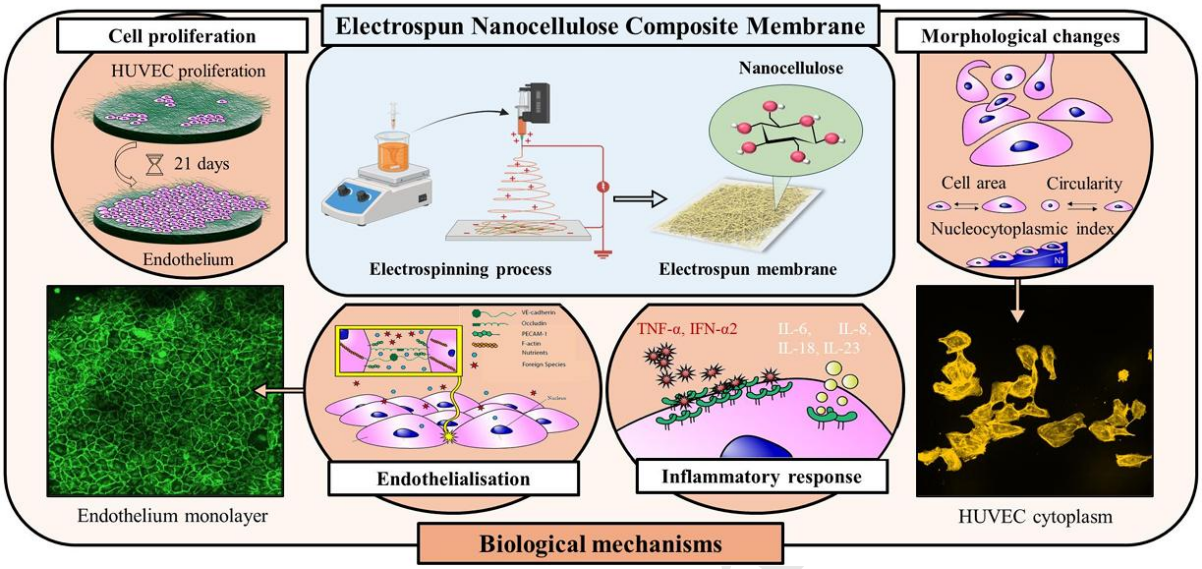

Highlights

- Electrospun nanocellulose composite membrane exhibits cytocompatibility with human umbilical vein endothelial cells (HUVECs).
- Both electrospun and solvent-casted nanocellulose derived membranes support endothelial cell attachment and proliferation for up to 21 days in culture.
- The fabrication strategy and resulting membrane physicochemical properties significantly influence endothelial cell responses and the kinetics of endothelialisation.
- Electrospun nanocellulose composite membrane demonstrate a more homogenous cytokine expression profile (IL-6, IL-23, IFN-α2, and TNF-α) during long-term culture, along with a progressive reduction in reactive oxygen species levels.
- These plant-derived nanocellulose biomaterials represent a sustainable platform for investigating endothelial cell-material interactions.